APPLIED PHYSICS

Emergent collective colloidal currents generated via exchange dynamics in a broken dimer state

Helena Massana-Cid[1]*, Antonio Ortiz-Ambriz[1,2]*, Andrej Vilfan[3,4], Pietro Tierno[1,2,5]†

Controlling the flow of matter down to micrometer-scale confinement is of central importance in material and environmental sciences, with direct applications in nano and microfluidics, drug delivery, and biotechnology. Currents of microparticles are usually generated with external field gradients of different nature (e.g., electric, magnetic, optical, thermal, or chemical ones), which are difficult to control over spatially extended regions and samples. Here, we demonstrate a general strategy to assemble and transport polarizable microparticles in fluid media through combination of confinement and magnetic dipolar interactions. We use a homogeneous magnetic modulation to assemble dispersed particles into rotating dimeric state and frustrated binary lattices, and generate collective currents that arise from a novel, field-synchronized particle exchange process. These dynamic states are similar to cyclotron and skipping orbits in electronic and molecular systems, thus paving the way toward understanding and engineering similar processes at different length scales across condensed matter.

INTRODUCTION

Confinement plays a central role in condensed matter physics (*1*), and it directly influences the transport properties of many systems, from electron flow in graphene (*2*) and heterostructure (*3*) devices to vortices in high-T_c superconductors (*4*), stochastic processes (*5*), and polymeric (*6*), glassy (*7*), and active matter (*8*) systems. In colloidal science, confining a suspension of microscopic particles between two flat surfaces reduces the overall mobility, screens electrostatics and hydrodynamics, and forces the dispersed particles to interact through excluded volume producing forms of aggregation otherwise unattainable (*9*). Confinement can also be used to measure colloidal interactions (*10*), probe the frictional deformations (*11*), or shed light on subtle effects such as critical Casimir forces (*12*). The combination of a confining mechanism with a predesigned interaction potential has been predicted to generate novel colloidal phases and dynamics (although no net current) (*13*–*15*), all phenomena impossible to observe in unconstrained systems. Despite the rapid progress in colloidal engineering, the few demonstrations of dispersion-free colloidal transport have been achieved only via specially prepared ferromagnetic substrates (*16*, *17*) requiring complex and often difficult fabrication procedures. Beyond such limitation, we show here that a combination of hard wall confinement and magnetic dipolar interactions generates colloidal states and currents that can be carefully controlled in situ by a homogeneous, time-dependent magnetic field.

RESULTS

Our system consists of an ensemble of paramagnetic colloidal particles with diameter $d = 2.8$ μm, dispersed in water and enclosed within a thin cell of thickness $h < 2d$ (Fig. 1, A to D; see Materials and Methods for more details). The system is quasi–two-dimensionally confined, and two particles can only pass each other by moving along the particle plane (unit vectors $\mathbf{e}_x$, $\mathbf{e}_y$), not jumping along the perpendicular ($\mathbf{e}_z$) direction. The particles are doped with nanoscale iron oxide grains, and they are responsive to an external magnetic field, $\mathbf{B}$. When $\mathbf{B} = 0$, they are unmagnetized and perform simple thermal diffusion along the same plane. Application of the external field induces a dipole moment $\mathbf{m} = \pi\chi d^3\mathbf{B}/(6\mu_0)$, where $\chi = 0.4$ is the magnetic volume susceptibility and μ_0 is the vacuum permeability. Pairs of particles (i, j) with moments $\mathbf{m}_{i,j} = m\mathbf{e}_{i,j}$ and at distance $r = |\mathbf{r}_i - \mathbf{r}_j|$ interact through dipolar forces, with an interaction potential given by $U_d(\mathbf{r}) = \omega\left[\frac{\mathbf{e}_i\cdot\mathbf{e}_j}{r^3} - \frac{3(\mathbf{e}_i\cdot\mathbf{r})(\mathbf{e}_j\cdot\mathbf{r})}{r^5}\right]$, with $\omega = \mu_0 m^2/(4\pi)$. This potential is maximally attractive (repulsive) for particles with magnetic moments parallel (perpendicular) to $\mathbf{r}$. In an unconstrained system, when the applied field is perpendicular to the particle plane, U_d reduces to an isotropic repulsion between parallel particles in the same plane, $U_d(r) = \omega/r^3$. This repulsion maximizes the interparticle distance, inducing the formation of a triangular lattice close to the bottom plate. Upon increasing $\mathbf{B}$, the strong dipolar repulsion may destabilize this structure, inducing out-of-plane motion and the assembly of particles into vertical columns (along $\mathbf{e}_z$) (*18*). The presence of confinement, however, softens the pair repulsion, avoiding the formation of these columns and leading to a different phase behavior (*19*). If we consider the particles between two hard walls at a distance $h < 2d$, the dipolar potential can be rewritten as $U_d(r,z) = \omega\frac{r^2-2z^2}{(r^2+z^2)^{5/2}}$. In this geometry, the particles repel when the elevation difference between their centers is $\Delta z < d/\sqrt{5}$, but otherwise, they experience a short-range attractive and long-range repulsive potential. Under a static field, it was shown that this change of the potential gives rise to different equilibrium phases characterized by a triangular, square, or labyrinthine type of ordering (*19*).

Instead of a static field, we drive the system out of equilibrium by using a time-dependent magnetic field, which performs a conical precession around $\mathbf{e}_z$,

$$\mathbf{B} = B_0[\cos\theta\mathbf{e}_z + \sin\theta(\cos(2\pi ft)\mathbf{e}_x + \sin(2\pi ft)\mathbf{e}_y)] \quad (1)$$

where f is the frequency and θ is the precession angle that we keep constant at 26.9°. The sequence of images in Fig. 1 (A to C) illustrates the impact of the magnetic precession on the particle aggregation process in

[1]Departament de Física de la Matèria Condensada, Universitat de Barcelona, 08028 Barcelona, Spain. [2]Institut de Nanociència i Nanotecnologia, Universitat de Barcelona, 08028 Barcelona, Spain. [3]Max Planck Institute for Dynamics and Self-Organization (MPIDS), 37077 Göttingen, Germany. [4]J. Stefan Institute, SI-1000 Ljubljana, Slovenia. [5]Universitat de Barcelona Institute of Complex Systems (UBICS), 08028 Barcelona, Spain.
*These authors contributed equally to this work.
†Corresponding author. Email: ptierno@ub.edu

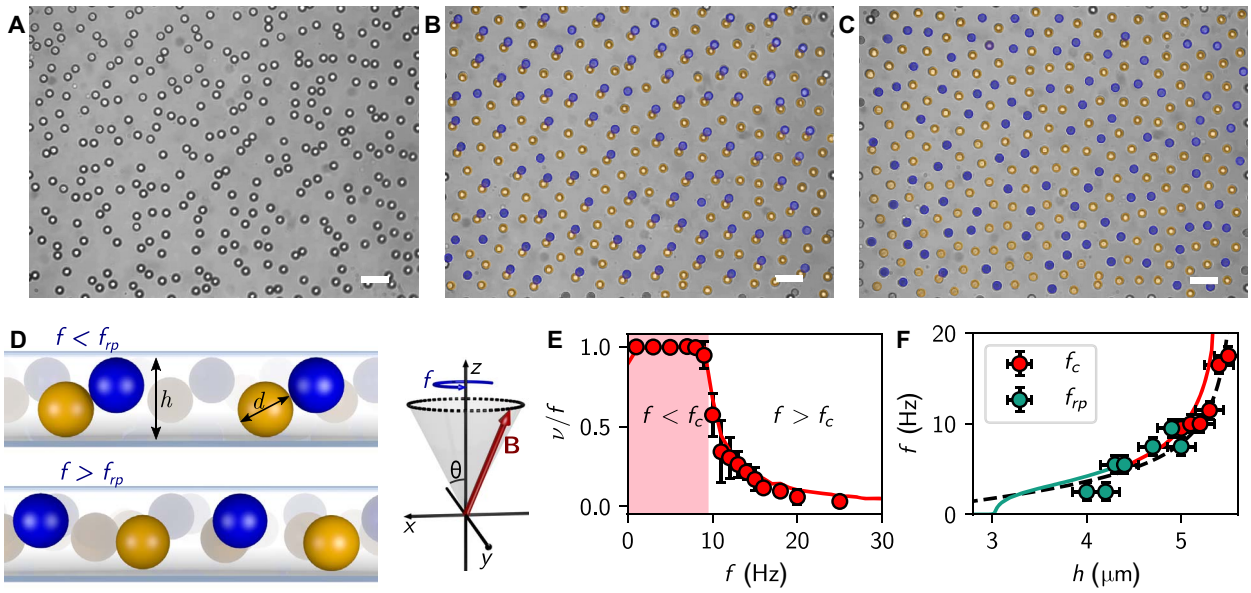

Fig. 1. Assembly procedure of colloidal dimers and binary lattices. (**A** to **C**) Microscope snapshots showing $N = 288$ particles in the absence of an external field (A) and driven by a precessing field with $B_0 = 7.3$ mT, $\theta = 26.9°$, and frequency $f = 1$ Hz (B) and $f = 20$ Hz (C). The dispersed particles (A) are first assembled to rotating dimers (B) and later broken into a binary arrangement of up and down particles (C) by raising f. For clarity, particles located close to the upper (lower) plate are shaded in blue (orange); the cell thickness is $h = 3.9$ μm. Scale bars, 10 μm for all images (movie S1). (**D**) Schematic showing the particle location inside a thin cell ($d < h < 2d$) when forming the dimers (top) and the up-down state (bottom). (**E** and **F**) Dynamics of single dimer: (E) cyclotron frequency ν of a dimer versus driving frequency f showing the transition from synchronous to asynchronous regime at $f_c = 9.8$ Hz from experiments (scattered data) and simulation (continuous line). In the synchronous phase, $\nu = f$, while above f_c the cyclotron rotation decreases following the equation $\nu = f - \sqrt{f^2 - f_c^2}$ (*24*). (F) Driving frequency versus confinement showing the transition of the dimers from synchronous to asynchronous (red, threshold at f_c) or from synchronous to rupture (green, threshold at f_{rp}). Experimental points are scattered data; theoretical model and simulations are represented by continuous and dashed lines, respectively.

a cell of thickness $h = 3.9$ μm. Starting from a disordered, fluid-like phase (Fig. 1A), the magnetic modulation assembles the dispersed particles into a lattice of rotating colloidal dimers, each performing a localized rotational motion around a common vertical axis (Fig. 1B). As shown in movie S1, the dimers behave as precessing tops, and the two particles display different brightness due to the differences in elevation (see also schematics in Fig. 1D). At low driving frequency, the cyclotron frequency ν of the spinning dimers is phase-locked with the driving field $\nu = f$.

This dynamic state may be changed by either raising f or varying the cell thickness h. For $h > 4.5$ μm, the spinning dimers transit from synchronous to asynchronous rotation (SA) above a critical frequency f_c, where the viscous torque overcomes the magnetic one and breaks the phase-locking (Fig. 1E). In this situation, the driving field rotates faster than the dimers and the phase-lag angle between the dimer director and **B** is no longer constant. The fast precession produces a characteristic "back-and-forth" dynamics during each field cycle and a reduction of the average cyclotron frequency. For stronger confinements ($h < 4.5$ μm), we observe that when f is higher than a threshold rupture frequency f_{rp}, there is a transition from the synchronous rotation to dimer rupture (SR), producing two separate lattices of up and down particles, as shown in Fig. 1C. Even if subjected to gravitational forces, the up particles remain stably located close to the upper surface as long as the magnetic field is applied. Similar to the buckled colloidal monolayer of compressed microgels particles (*9*), the up-down state can be mapped to a frustrated Ising antiferromagnet on a triangular lattice (*20*). However, our lattice features a much larger interparticle distance, which results from the softness of the pair potentials.

DISCUSSION

To predict the dynamic states formed by the magnetic dimers at low density, we develop a physical model based on the balance between the magnetic torque τ_m required to rotate the dimer (eq. S2) and the viscous one τ_ν, which arises from the rotation in the fluid (eq. S4). The main result is the rotation frequency function

$$\nu = \nu_0 \frac{\sin\theta}{\sin\alpha} \sin\phi \,(\sin\alpha \sin\theta \cos\phi + \cos\alpha \cos\theta) \qquad (2)$$

where α is the minimum angle between the center to center vector joining two particles and the vertical axis, ϕ is the angle between the horizontal projections of the magnetic field and the dimer orientation, $\nu_0 = \frac{\chi^2 B^2 d}{24\mu_0\gamma} \sim 14.4$ Hz, and γ is the viscous drag coefficient of the particle. The maximum rotation frequency f_c is determined by the maximal value of ν(ϕ). Above f_c, synchronous rotation is not possible and phase slippage occurs. Alternatively, the dimer can rupture at a lower frequency f_{rp}. The resulting frequencies, f_c and f_{rp}, are compared with experimental values in Fig. 1F. Even if this analysis only considers the stability of individual dimers, it captures well the dynamics of the ensemble at low densities, due to the large interparticle distance. The single dimer stability analysis is shown in figs. S1 and S2.

Increasing the particle density forces the dimers to interact, producing collective states where they can break up, and their components exchange position with other particles in nearest dimers. Experiments and numerical simulations (see Materials and Methods) are used in tandem to unveil the rich dynamic paths that arise by changing h and the

normalized area packing fraction, $\Phi = N\pi d^2/(4A)$, where N is the number of particles and A is the observation area. The colored arrows in Fig. 2A summarize the four situations encountered, while the diagram in Fig. 2B shows the good agreement between the experimental data (scattered points) and the numerical simulations (shaded regions). In all cases, we start from an ensemble of spinning dimers in the synchronous state. We find that for packing fraction $\Phi > 0.35$, the SA and SR transitions display an intermediate exchange state, which gives rise to the synchronous-exchange-asynchronous (SEA) and synchronous-exchange-rupture (SER) regimes.

We characterize these regimes by measuring the average cyclotron frequency (Fig. 2C) and the average distance $\langle \Delta r \rangle$ between nearest neighbors (Fig. 2D). The first observable shows that the SA regime (orange line) can be described by the single dimer behavior, fitting the curve with the function $\nu = \nu(f)$ in caption of Fig. 1, while the SEA (red line) shows a large deviation after the synchronous state. The other two states, SR and SER, disappear quickly after the synchronous state because they show no stable dimers. Thus, we use the second observable, shown in Fig. 2D, to characterize these regimes. For a system in the SA regime, the average distance has a constant plateau with $\langle \Delta r \rangle \approx d$ because the dimers do not break but simply slow down their orbital motion. In contrast, $\langle \Delta r \rangle$ reaches the maximum value for the SR path, when the colloids form the up and down lattice. The SEA and SER states are observed at higher packing fraction, which corresponds to a lower separation distance. In the SEA regime, $\langle \Delta r \rangle$ momentarily increases above d before falling back when the system returns to an asynchronous rotation. While the SR regime shows a quick transition to its maximum distance, the SER displays an intermediate region where the average distance depends linearly with the frequency.

For an isotropic precessing field, the exchange events occur randomly through the sample and arise from a spontaneous dynamical symmetry breaking process. We create a polarized bidirectional colloidal current by imposing a small in-plane field B_s that breaks the spatial isotropy of the precession. The result of this bias is a synchronized bidirectional flux of particles where the up and down paramagnetic colloids periodically separate and recombine, as shown in Fig. 3 (A and B) and movie S3. We quantify the amplitude of this current by measuring the mean velocity v_e of particle i at elevation z_i from the middle plane as $\mathbf{v}_e = \langle (v_{y,i}\mathbf{e}_x - v_{x,i}\mathbf{e}_y) z_i / |z_i| \rangle$ (Fig. 3C). This expression averages the in-plane velocity components of all particles, giving the same sign to opposite propelling particles located on different planes. The colloidal current normalized to the maximum particle velocity is thus given by $I = 2|v_e|/(fd\sqrt{\frac{\pi}{\sqrt{3}\Phi}})$. The maximum current $I = 1$ corresponds to the fully synchronized transport, where all particles travel one lattice site per field cycle. Figure 3C shows the colloidal current versus shift angle δ for different frequencies. For high f (blue lines), the current increases slowly with δ; the system is initially in an asynchronous state with few exchange events that increase in probability with higher bias. In contrast, at low f (red lines), there is no initial current for low δ, and the system starts from a synchronous state. Above a critical bias, the events of particle exchange become directional, and

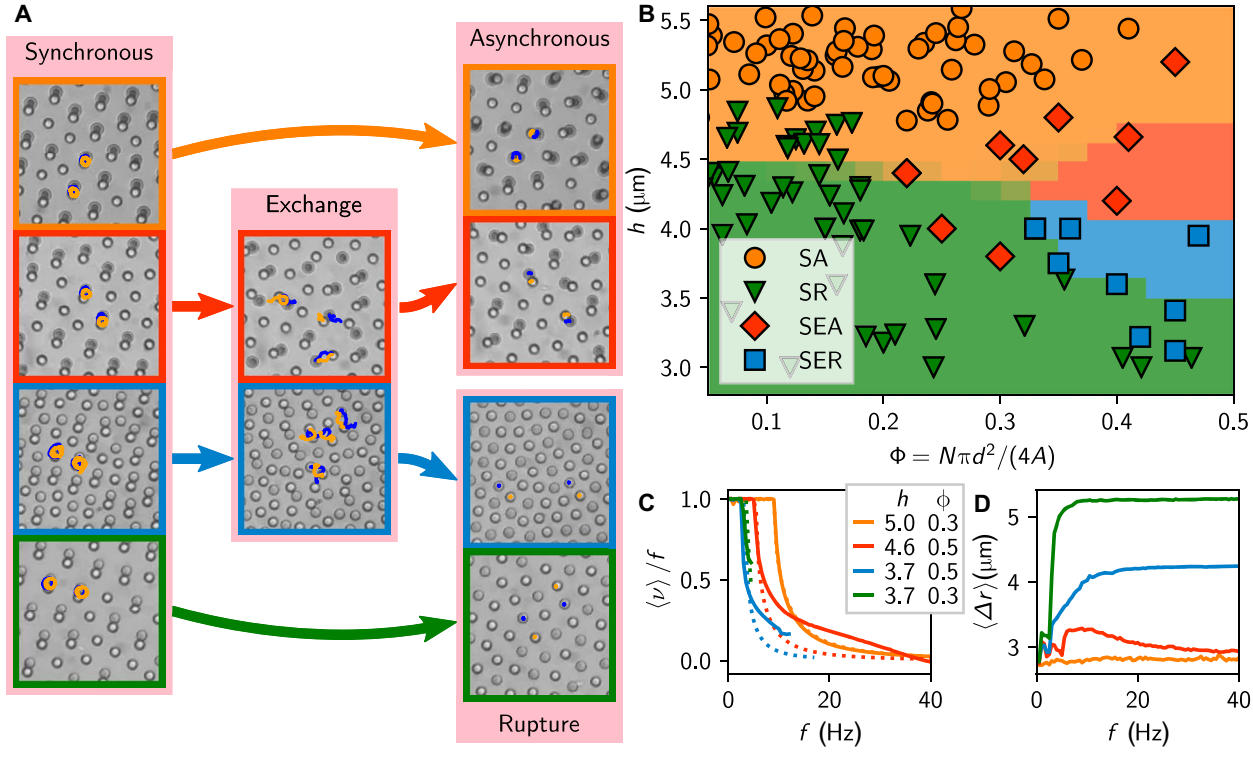

Fig. 2. Dynamic colloidal states from experiments and numerical simulations. (**A**) Images illustrating different transition paths observed for B_0 = 7.28 mT, θ = 26.9°; all starting from a synchronous orbit at f = 1 Hz. SA: Synchronous → Asynchronous rotations (f = 20 Hz), h= 5.1 μm; SEA: Synchronous → Exchange of neighbors (f = 8 Hz) → Asynchronous (f = 25 Hz), h = 4.4 μm; SER: Synchronous → Exchange of neighbors (f = 3 Hz) → Rupture (f = 14 Hz), h = 4.4 μm; SR: Synchronous → Rupture (f = 9 Hz), h = 4.0 μm (movie S2). (**B**) Combined experiment (symbols) and simulation (colored regions) results of the location of the different transition paths in the (Φ, h) plane. (**C** and **D**) From simulations: Average cyclotron frequency of the dimers ν (C) and nearest neighbor separation distance $\langle \Delta r \rangle$ (D) versus driving frequency f. Both quantities can be used to classify the different transition paths observed.

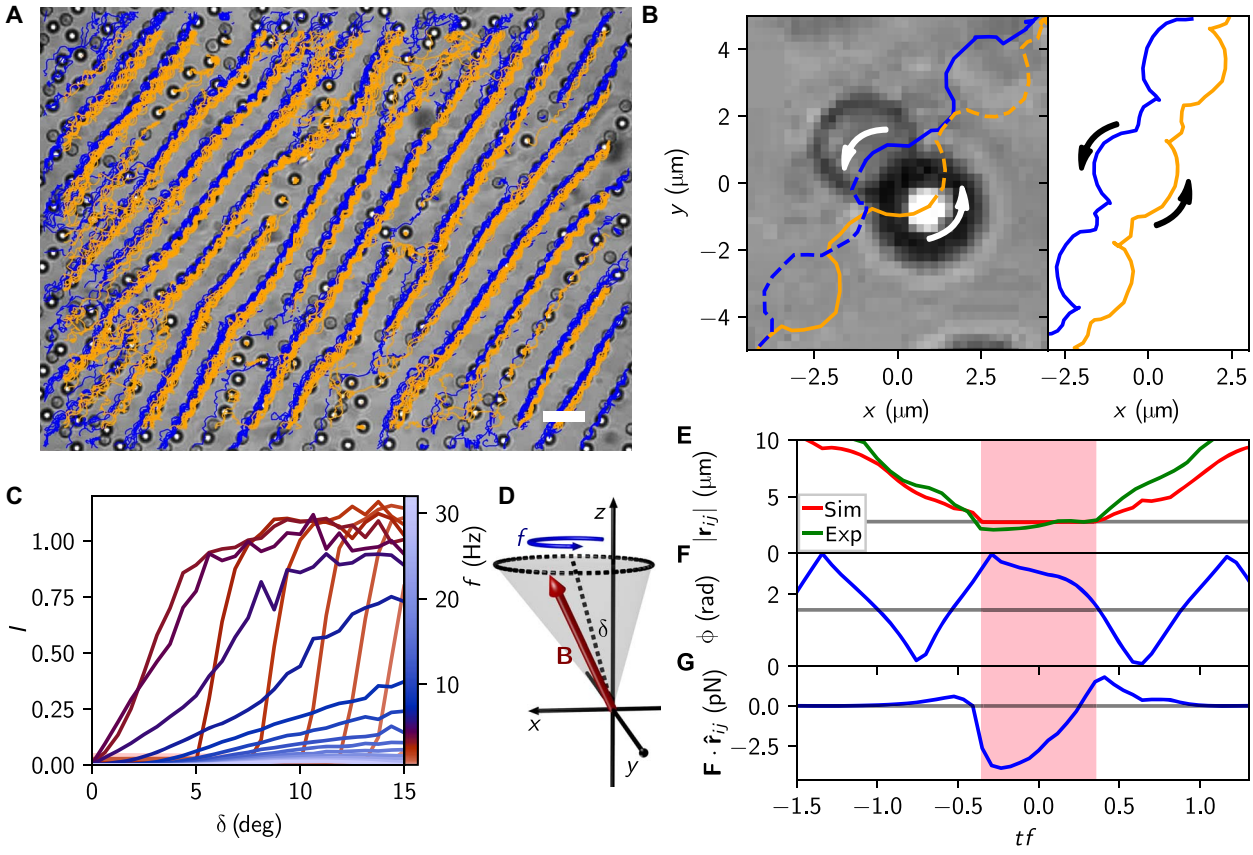

Fig. 3. Colloidal current. (**A**) Microscope image with superimposed trajectories of up (blue) and down (orange) particles driven by an off-axis precessing field with B_0 = 7.2 mT, θ = 26.9°, and f = 6 Hz in a cell of thickness h = 4 μm (movies S3 and S4). Scale bar, 10 μm. (**B**) Enlargement of this image with only two superimposed particle trajectories from experiments (left) and simulation (right). (**C**) Intensity I of the colloidal current versus shift angle δ for different values of the driving frequency (color bar) from simulations. High frequencies (blue lines) produce a smooth raise of I to the maximum flow, where all up and down particles contribute to the current. For f < 4 Hz (red lines), we observe a sharp increase from zero current to the maximum value at a fixed δ. (**D**) Schematic showing a shifted conical field obtained by adding a zenithal angle δ, which only rotates the static component of the magnetic field, $\mathbf{B}_s$ = sin (δ)$\mathbf{e}_x$+ cos (δ)$\mathbf{e}_z$. With this additional bias, the external field now reads as $\mathbf{B}(t) = B_0[($ sin (θ) cos (2πft) + cos (θ) sin (δ))$\mathbf{e}_x$ + sin (θ) sin (2πft)$\mathbf{e}_y$ + cos (θ) cos (δ)$\mathbf{e}_z$]. (**E** to **G**) Details on the exchange mechanism: (E) interparticle distance r_{ij} between two particles (i,j), from experiments and simulations. Only from simulations: (F) phase lag angle between the dimer and the field ϕ and (G) projection of the magnetic dipolar force $F \cdot \hat{r}_{ij}$ versus rescaled time t. The pink shaded region indicates the time window of the dimer formation, $r_{ij} = 2d$.

the system quickly reaches the maximum current. The emergence of the colloidal current I can be understood by carefully analyzing the exchange and recombination process of two particles in Fig. 3 (B, E, and F). When two approaching up and down particles are pushed close to each other by the repulsion from their neighbors, their dipolar interaction is first repulsive, but it quickly becomes attractive, creating a new dimer (pink region in Fig. 3, E and F). However, the viscous torque impedes the dimer to rotate as fast as the field. This effect appears in Fig. 3F, where the in-plane angle between the field and the dimer director is not constant but decreases with time starting from ϕ = π. When the relative angle becomes close enough to π/2, the dipole moments are parallel and the dipolar force becomes repulsive. Now, the dimer breaks and the composing particles are pushed apart, coupling to the next particle of the lattice in a minuet type of motion. The result is a bidirectional current of up and down particles that flow along the same direction but in opposite sense. Thus, our numerical simulations demonstrate that the colloidal transport arises only from the combined action of confinement and dipolar forces, without considering any hydrodynamic effect or rotational motion of the particles close to the surface. We note that, within the narrow space of widths where the system can be considered quasi–two-dimensional ($d < h < 2d$), the particle current was observed in a range of widths $h \in$ [3.5,4.5]μm. Experimentally, we find that reducing further the cell thickness (h < 3.5 μm) would impede the formation of the dimeric state and thus the particle flow. On the other hand, increasing the size of the cell would create vertical dimers, with very small rotational precession increasing their pair separation and avoiding the exchange process to take place. Further, we used numerical simulations to test how stable our transport mechanism is against reduction of the sample area, in particular for the case of a narrow slit. As shown in movie S5, even in this situation, we find that it is possible to reproduce the exchange dynamics and the bidirectional particle flow, which opens the door toward potential applications of our method in narrow microfluidic channels and pores.

In conclusion, we have shown that the combination of confinement and time-dependent magnetic fields produces a rich repertoire of dynamic states starting from a population of inert colloidal spheres. We realize self-assembled dimers with localized orbital motion, frustrated binary lattices, and robust bidirectional currents. This transport dynamics resembles the skipping orbits in a dilute electron gas moving through semiconductor heterostructures (*21*), inviting a fundamental study of

the analogy between both processes at a semiclassical level. The exotic states we report here via an engineered soft-shoulder potential were predicted in different theoretical models, but not observed so far (*13*, *15*). We note that similar dynamic states with particles sliding in opposite directions have been recently observed in a numerical simulation of bidisperse spinning particles with a dispersion in the Magnus term (*22*). Our results also open a new avenue in manipulation of microscopic matter in fluids, with great potential for noninvasive transport of colloidal matter through small membranes and pores, where confinement plays a key role.

MATERIALS AND METHODS

Experimental details

We use paramagnetic colloidal particles composed of a cross-linked polystyrene matrix with surface carboxylic groups (Dynabeads M-270, Invitrogen). The particles have a narrow size distribution (coefficient of variation < 3%) and are doped with ferrite (~20%), which gives a density $\rho = 1.6$ g/cm^3. The particle stock solution is sandwiched between two glass surfaces. The confinement cell is constructed by using a plain microscope slide (thickness, 0.9 to 1.06 mm; Corning) and a coverslip (no. 1, Thermo Scientific Menzel). Both plates are manually pressed and glued along two sides with a fast-curing epoxy adhesive. By varying the applied pressure between the plates, it was possible to obtain a confinement ranging from 3 to 6 μm. The remaining two sides of the cell are sealed after the particle suspension is inserted by capillary action.

The cell is placed on the stage of an upright optical microscope (Eclipse Ni, Nikon). The particle dynamics are observed via a charge-coupled device camera (Scout scA640-74f, Basler) operating at 75 frames per second. The applied magnetic fields are generated using a set of three perpendicular custom-made magnetic coils. The rotating in-plane component is obtained by connecting two coils ($\mathbf{e}_x$, $\mathbf{e}_y$) to a power amplifier (DAP Palladium P-400, Vintage) controlled via a waveform generator (TGA1244, TTi). The field rotation is obtained by programming two sinusoidal currents with $\pi/2$ phase shift along these two coils. The precessing field is then obtained by adding a static field along the vertical axis ($\mathbf{e}_z$), which is generated with the third coil connected to a DC power supply (EL302RT, TTi).

The cell height h is measured in the following manner. In a confined dispersion of particles, a DC field along the $\mathbf{e}_z$ direction is applied to form isolated dimers. From a set of microscope snapshots, the horizontal projection length of the dimers was determined via image analysis, and the elevation h was extracted.

Numerical simulation

Brownian dynamics simulations were performed using the free package LAMMPS (*23*), modified to include an overdamped integrator and an induced dipole moment of the particles. The modified code can be found at http://github.com/aortiza/lammps. We consider N paramagnetic colloids at positions $r_i \equiv (x_i, y_i, z_i)$. To fix a packing fraction, we set periodic boundary conditions in the ($\mathbf{e}_x$, $\mathbf{e}_y$) plane, while z_i is constrained by placing two hard walls at positions $\pm h/2$. We integrate the overdamped equation of motion

$$\gamma \frac{d\mathbf{r}_i}{dt} = \sum_{j \neq i} \mathbf{F}_{\text{int}}(\mathbf{r}_i - \mathbf{r}_j) + \mathbf{F}_w + \mathbf{F}_g + \boldsymbol{\eta}(t) \tag{3}$$

where γ is the viscous friction, $\mathbf{F}_{\text{int}}(\mathbf{r}_i - \mathbf{r}_j)$ is the total force exerted on particle i by particle j, $\mathbf{F}_w$ is the normal force exerted by the walls on particle i, and $\mathbf{F}_g$ is the gravitational force. The first term can be written as $\mathbf{F}_{\text{int}}(\mathbf{r}_i - \mathbf{r}_j) = -\nabla U_{\text{int}}(\mathbf{r}_i - \mathbf{r}_j)$, where the interactions between the particles are given by the dipolar term (see the main text) with the addition of a repulsive Weeks-Chandler-Andersen (WCA) potential U_{WCA}, $U_{\text{int}}(\mathbf{r}_i - \mathbf{r}_j) = U_d(\mathbf{r}_i - \mathbf{r}_j) + U_{\text{WCA}}(|\mathbf{r}_i - \mathbf{r}_j|)$. In the calculation of the dipole-dipole interaction, we take into account the contribution of the magnetic field produced by nearest particles. This is calculated iteratively, and we find that typically only two iterations for the dipole moments were enough to converge. Thus, to speed up the simulations, we set up a cutoff for the magnetic interaction of ~30 μm. The WCA potential is given by

$$U_{WCA}(r) = \begin{cases} 4\epsilon\left[\left(\frac{d}{r}\right)^{12} - \left(\frac{d}{r}\right)^{6}\right] + \epsilon & r < 2^{\frac{1}{6}}d \\ 0 & r > 2^{\frac{1}{6}}d \end{cases} \tag{4}$$

The interaction force between particle i and the walls is given by $\mathbf{F}_w(z) = -\nabla U_w(z)$, where $U_w(z)$ is also approximated by a WCA potential

$$U_w(z) = \begin{cases} 4\epsilon\left[\left(\frac{\frac{d}{2}}{z+\frac{h}{2}}\right)^{12} - \left(\frac{\frac{d}{2}}{z+\frac{h}{2}}\right)^{6}\right] + \epsilon & z < \left(\frac{d}{2^{5/6}} - \frac{h}{2}\right) \\ 0 & \text{elsewhere} \\ 4\epsilon\left[\left(\frac{\frac{d}{2}}{z-\frac{h}{2}}\right)^{12} - \left(\frac{\frac{d}{2}}{z-\frac{h}{2}}\right)^{6}\right] + \epsilon & z > \left(\frac{h}{2} - \frac{d}{2^{5/6}}\right) \end{cases} \tag{5}$$

The gravitational force is given by $\mathbf{F}_g = -\Delta\rho V g z$, where g is the gravitational acceleration, V is the particle volume, and $\Delta\rho$ is the density mismatch between the particle and water. Last, $\boldsymbol{\eta}(t) \equiv (\eta_x, \eta_y, \eta_z)$ in Eq. 3 are random Gaussian variables with mean $\langle \eta_i(t) \rangle = 0$ and correlation function $\langle \eta_i(t)\eta_j(t') \rangle \equiv 2k_B T\gamma\delta_{ij}\delta(t - t')$, where T is the temperature and k_B is the Boltzmann constant.

We numerically integrate Eq. 3 using a finite time step of $\Delta t = 10^{-4}$s and use experimental parameters for most quantities ($\gamma = 56.74 \times 10^{-6}$pN s nm^{-1}, $\Delta\rho = 10^3$kg m^{-3}, $g = 9.8$ m s^{-2}, and $\epsilon = 10^4$pN nm).

SUPPLEMENTARY MATERIALS

Supplementary material for this article is available at http://advances.sciencemag.org/cgi/content/full/6/10/eaaz2257/DC1

Single dimer stability analysis

Fig. S1. Schematics showing a magnetic dimer in confinement.

Fig. S2. Dynamical phases of a single magnetic dimer in a precessing field.

Movie S1. Experimental realization of colloidal dimers and binary crystals.

Movie S2. Different dynamic states of confined colloidal dimers under precessing field.

Movie S3. Colloidal current generated by a precessing field.

Movie S4. Trajectories of two particles producing the bidirectional current.

Movie S5. Bidirectional colloidal current in a narrow slit from simulation.

REFERENCES AND NOTES

1. L. D. Gelb, K. E. Gubbins, R. Radhakrishnan, M. Sliwinska-Bartkowiak, Phase separation in confined systems. *Rep. Prog. Phys.* **62**, 1573–1659 (1999).
2. A. H. Castro Neto, F. Guinea, N. M. R. Peres, K. S. Novoselov, A. K. Geim, The electronic properties of graphene. *Rev. Mod. Phys.* **81**, 109–162 (2009).

3. C. Gong, X. Zhang, Two-dimensional magnetic crystals and emergent heterostructure devices. *Science* **363**, eaav4450 (2019).
4. G. Blatter, M. V. Feigel'man, V. B. Geshkenbein, A. I. Larkin, V. M. Vinokur, Vortices in high-temperature superconductors. *Rev. Mod. Phys.* **66**, 1125–1388 (1994).
5. T. Guérin, N. Levernier, O. Bénichou, R. Voituriez, Mean first-passage times of non-Markovian random walkers in confinement. *Nature* **534**, 356–359 (2016).
6. S. Zhu, Y. Liu, M. H. Rafailovich, J. Sokolov, D. Gersappe, D. A. Winesett, H. Ade, Confinement-induced miscibility in polymer blends. *Nature* **400**, 49–51 (1999).
7. E. Flenner, G. Szamel, Fundamental differences between glassy dynamics in two and three dimensions. *Nat. Commun.* **6**, 392 (2015).
8. A. Bricard, J. B. Caussin, N. Desreumaux, O. Dauchot, D. Bartolo, Emergence of macroscopic directed motion in populations of motile colloids. *Nature* **503**, 95–98 (2013).
9. Y. Han, Y. Shokef, A. M. Alsayed, P. Yunker, T. C. Lubensky, A. G. Yodh, Geometric frustration in buckled colloidal monolayers. *Nature* **456**, 898–903 (2008).
10. Y. Liang, N. Hilal, P. Langston, V. Starov, Interaction forces between colloidal particles in liquid: Theory and experiment. *Adv. Colloid Interf. Sci.* **134–135**, 151–166 (2007).
11. T. Bohlein, J. Mikhael, C. Bechinger, Observation of kinks and antikinks in colloidal monolayers driven across ordered surfaces. *Nat. Mater.* **11**, 126–130 (2011).
12. C. Hertlein, L. Helden, A. Gambassi, S. Dietrich, C. Bechinger, Direct measurement of critical Casimir forces. *Nature* **451**, 172–175 (2008).
13. P. J. Camp, Structure and phase behavior of a two-dimensional system with core-softened and long-range repulsive interactions. *Phys. Rev. E* **68**, 061506 (2003).
14. C. Reichhardt, C. J. Olson, Novel colloidal crystalline states on two-dimensional periodic substrates. *Phys. Rev. Lett.* **88**, 248301 (2002).
15. J. Dobnikar, J. Fornleitner, G. Kahl, Ground states of model core-softened colloids. *J. Phys. Condens. Matter* **20**, 494220 (2008).
16. B. B. Yellen, O. Hovorka, G. Friedman, Arranging matter by magnetic nanoparticle assemblers. *Proc. Natl. Acad. Sci. U.S.A.* **102**, 8860–8864 (2005).
17. P. Tierno, F. Sagués, T. H. Johansen, T. M. Fischer, Colloidal transport on magnetic garnet films. *Phys. Chem. Chem. Phys.* **11**, 9615–9625 (2009).
18. Y. H. Miao, D. L. Geng, L. E. Helseth, Order–disorder transition in a quasi-two-dimensional colloidal system. *Langmuir* **22**, 5572–5574 (2006).
19. N. Osterman, D. Babič, I. Poberaj, J. Dobnikar, P. Ziherl, Observation of condensed phases of quasiplanar core-softened colloids. *Phys. Rev. Lett.* **99**, 248301 (2007).
20. G. H. Wannier, Antiferromagnetism. The triangular ising net. *Phys. Rev.* **79**, 357–364 (1950).
21. C. W. J. Beenakker, H. van Houten, B. J. van Wees, Skipping orbits, traversing trajectories, and quantum ballistic transport in microstructures. *Superlattice. Microst.* **5**, 127–132 (1989).
22. C. J. O. Reichhardt, C. Reichhardt, Disordering, clustering, and laning transitions in particle systems with dispersion in the Magnus term. *Phys. Rev. E* **99**, 012606 (2019).
23. S. Plimton, Fast parallel algorithms for short-range molecular dynamics. *J. Comput. Phys.* **117**, 1–19 (1995).
24. A. Cēbers, M. Ozols, Dynamics of an active magnetic particle in a rotating magnetic field. *Phys. Rev. E* **73**, 021505 (2006).

Acknowledgments: We thank F. Martinez-Pedrero for initial experiments and T. M. Fischer and Y. Shokef for stimulating discussions. **Funding:** H.M.-C., A.O.-A., and P.T. acknowledge support from the European Research Council (grant agreement no. 811234). A.V. acknowledges support from the Slovenian Research Agency (grant P1-0099). P.T. acknowledges support from MINECO under projects FIS2016-78507-C2-2-P and ERC2018-092827 and Generalitat de Catalunya under project 2017SGR1061 and programa "ICREA Acadèmia." **Author contributions:** H.M.-C. performed the experiments. A.O.-A. performed the numerical simulations. A.V. developed the theoretical model. P.T. supervised the work and wrote the paper. All the authors discussed and interpreted the results. **Competing interests:** The authors declare that they have no competing interests. **Data and materials availability:** All data needed to evaluate the conclusions in the paper are present in the paper and/or the Supplementary Materials. Additional data related to this paper may be requested from the authors.

Submitted 22 August 2019
Accepted 12 December 2019
Published 6 March 2020
10.1126/sciadv.aaz2257

Citation: H. Massana-Cid, A. Ortiz-Ambriz, A. Vilfan, P. Tierno, Emergent collective colloidal currents generated via exchange dynamics in a broken dimer state. *Sci. Adv.* **6**, eaaz2257 (2020).

Emergent collective colloidal currents generated via exchange dynamics in a broken dimer state

Helena Massana-Cid, Antonio Ortiz-Ambriz, Andrej Vilfan and Pietro Tierno

Sci Adv **6** (10), eaaz2257.
DOI: 10.1126/sciadv.aaz2257